Chen W, Zheng L, Huo D, Chen Y.

Surface texture formation by non-resonant vibration assisted micro milling.

***Journal of Micromechanics and Microengineering* 2018, 28(2), 025006**

Surface texture formation by non-resonant vibration assisted micro milling

Wanqun Chen[1,2], Lu Zheng[1], Dehong Huo[1*], Yiwu Chen[3]

1.Mechanical Engineering, School of Engineering, Newcastle University, Newcastle upon Tyne, NE1 7RU, UK

2.Center for Precision Engineering, Harbin Institute of Technology, Harbin 150001, P. R. China

3.School of Mechanical and Systems Engineering, Nanjing University of Aeronautics and Astronautics, Nanjing 210016, P. R. China

[*]Corresponding author: D. Huo, Tel: +44 (0) 191 208 6230, E-mail: dehong.huo@newcastle.ac.uk

Abstract: This paper proposes a new surface texture formation method by non-resonant vibration assisted milling. Firstly, the kinematics of vibration assisted milling process is formulated and surface texture formation in end milling with different machining and vibration parameters is discussed. Various types of surface textures can be generated by different combination of machining and vibration parameters. Secondly, a novel 2D non-resonant vibration stage is developed to realize the vibration during the milling process. Thirdly, vibration assisted milling experiments are carried out to verify the proposed surface texture formation method and the effects of the vibration and machining parameters on the surface texture generation. Finally, hydrophilic performance of the machined surfaces with different surface textures is investigated to demonstrate the application of the proposed method.

Keywords: vibration assisted machining; vibration assisted milling; surface texture; vibration stage design; hydrophilicity

1. Introduction

Engineered textured surfaces have the characteristics of regular texture structure and high aspect ratio, enabling the component surface to have superior properties, such as reducing adhesion friction [1], improving lubricity [2], increasing wear resistance [3], changing the hydrophilic performance [4], and enhancing optical properties [5]. Such advantages are widely used for numerous applications, such as sliding contact elements, magnetic storage disk surfaces, machine tool guideways, hydrodynamic bearings, cam followers, rolls of forming processes, and mechanical face seals [6,7]. Therefore, it is of great significance to investigate and manufacture engineered surface textures. At present micro surface texture manufacturing methods contain MEMS technology [8-11], e.g. Lithography, chemical etching, LIGA; energy beam processing technology [12-14], e.g. laser beam machining, Ion beam machining; electro discharge machining [15]; ultra-precision machining technologies [16-18], e.g. fly-cutting, turning, micro milling. While, these micro structure machining methods have some drawbacks, such as high cost, low efficiency, serious environmental pollution. Vibration assisted machining, initially developed to improve machinability of hard-to-machine materials, has shown its capacity in generating surface texture. Surface texture generation by vibration assisted milling, as a newly emerged method, can generate certain surface textures on the machined surface at a more efficient manner. This paper presents numerical modelling of cutting trajectories in vibration assisted milling (VAMILL) and proposes a novel method to obtain surface textures by non-resonant vibration assisted milling. There are two working modes of vibration stage design: resonant mode and non-resonant mode vibration. Resonant mode vibration systems are capable of working at higher operating frequency and is more energy efficient, but they can

only work at certain discrete frequencies. Non-resonant mode vibration systems are typically implemented using the piezo-actuator driven flexure mechanism, and can work at a large range of continuous operating frequencies and offers a more precise motion control. This study investigates surface texture generation using non-resonant mode vibration assisted milling.

2. Numerical simulation of vibration assisted milling

2.1 Kinemics analysis of vibration assisted milling

In VAMILL, high frequency and small amplitude vibration can be superimposed to either the tool or the workpiece side. According to the dimension of the vibration applied, vibration assisted milling can be divided into two groups: 1D and 2D vibration assistance. In 1D VAMILL, vibration is applied either in the feed direction, feed-directional vibration assisted milling (FVAMILL), or in the cross-feed direction, cross-feed-directional vibration assisted milling (CFVAMILL). In 2D VAMILL, vibrations are applied simultaneously in both the feed and the cross-feed directions (2DVAMILL). Fig. 1 shows a schematic diagram of vibration assisted milling. The coordinate system used in this paper is defined as follows: the workpiece feed is in x direction; the cross-feed direction is in y direction, and axial depth of cut is in z direction.

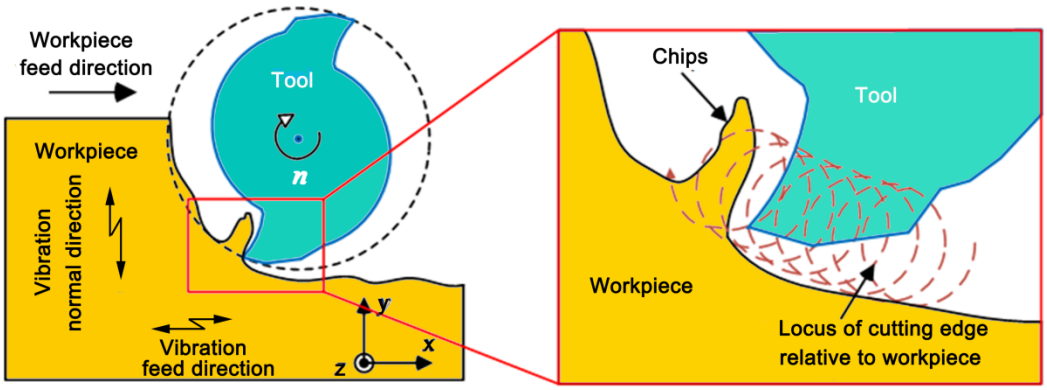

Fig. 1 Schematic of vibration assisted milling

The mathematical equation of the tool tip motion, (x, y), without vibration imposed is as follows:

$$\begin{cases} x = r\sin\left[\omega t - \dfrac{2\pi\left(z_i - 1\right)}{Z}\right] \\ y = r\cos\left[\omega t - \dfrac{2\pi\left(z_i - 1\right)}{Z}\right] \end{cases} \tag{1}$$

where, r and ω are the radius and angular velocity of the cutter, respectively. z_i is the i^{th} cutter tooth, and Z is number of flutes.

Assume that vibration is applied to workpiece and the vibration trajectory of the tool tip is as follows:

$$\begin{cases} x_w = ft + A\sin\left(2\pi f_x t + \phi_x\right) \\ y_w = B\sin\left(2\pi f_y t + \phi_y\right) \end{cases} \tag{2}$$

where f is feed velocity, A and B are the vibration amplitudes, f_x and f_y are the vibration frequencies, ϕ_x and ϕ_y are the phase angles, in x and y directions, respectively. The relative displacement (x_i, y_i) of tool tip to workpiece in VAMILL can be obtained from Eq.(1-2):

$$\begin{cases} x_i = ft + r\sin\left[\omega t - \dfrac{2\pi\left(z_i - 1\right)}{Z}\right] + A\sin\left(f_x t + \phi_x\right) \\ y_i = r\cos\left[\omega t - \dfrac{2\pi\left(z_i - 1\right)}{Z}\right] + B\sin\left(f_y t + \phi_y\right) \end{cases} \tag{3}$$

2.2 Surface texture generation simulation

The vibration applied in the feed direction is investigated in this paper. As the applied vibration trajectory is a sinusoidal curve, the phase difference between adjacent tool trajectories determines the surface texture generated. There are two typical tool trajectories for the vibration assisted milling: one is wave type tool trajectory when the crests (valleys) of the current cutter

trajectory corresponds to crests (valleys) of the following tool trajectory as shown in Fig.2 (a); another is fish scale tool trajectory when the crests (valleys) of the current cutter trajectory corresponds to valleys (crests) of the following cutter trajectory, as shown in Fig.2 (b).

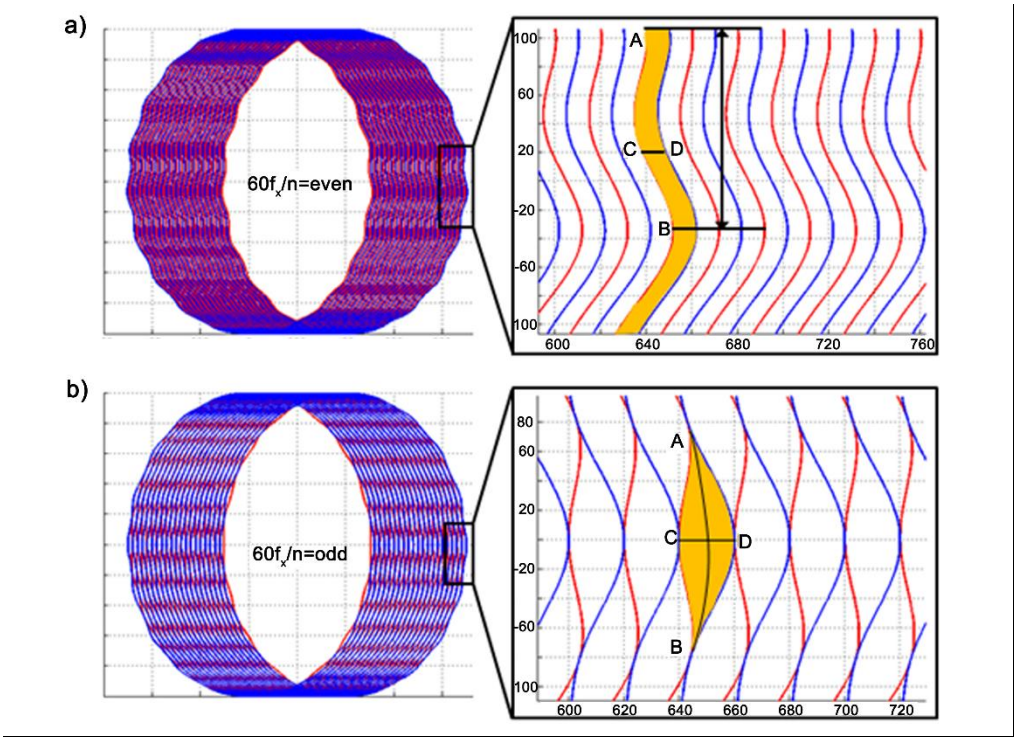

Fig. 2 Two typical trajectories of vibration assisted milling, a) wave tool trajectory, b) fish scale tool trajectory

As the two tool trajectories are determined by the phase difference between adjacent tool trajectories, and the tool trajectories are influenced by the ratio between the vibration frequency and the spindle rotation frequency. There exist two cases to generate the above-mentioned two typical tool trajectories. The conditions are discussed as follows:

$$60f_x/n = \begin{cases} \text{even}, & \text{Wave tool trajectory appears} \\ \text{odd}, & \text{Fish scales tool trajectory appears} \end{cases} \quad (5)$$

where f_x is the vibration frequency in x direction, Hz;

n is the spindle speed, rpm.

Since two flute tools are widely used in micro milling, the following discussion is based on micro end mills with two teeth. When the ratio between the vibration frequency and the spindle rotation frequency is an odd value, the 1st case occurs and generates a wave surface texture as shown in Fig.2 (a). The characteristic dimensions AB and CD can be expressed in terms of spindle rotation and vibration frequency.

$$\begin{cases} \widehat{AB}=\pi rn/60f_x \\ CD=f_z \end{cases} \quad (6)$$

When the ratio between vibration frequency and spindle rotation frequency is an even value, there are three typical fish scale type surface textures, as shown in Fig.3. When $A < f_z/2$, the adjacent tool trajectories fluctuate but do not intersect, which forms the first type of fish scale surface texture as shown in Fig. 3 (a). The characteristic dimensions can be obtained as:

$$\begin{cases} \widehat{AB}=\pi rn/60f_x \\ CD=2A_x \end{cases} \quad (7)$$

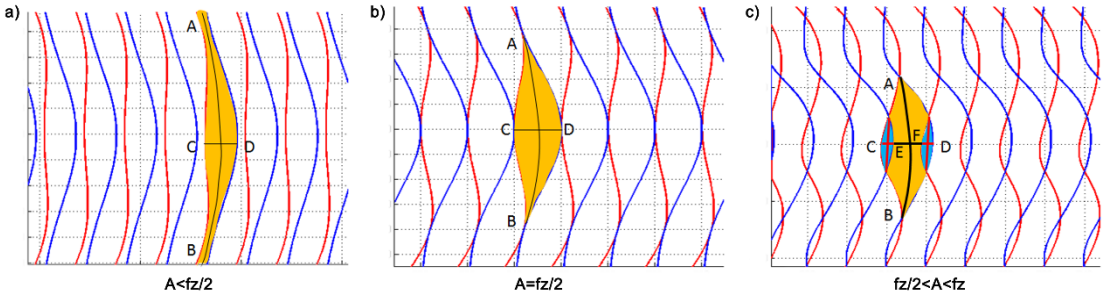

Fig.3 Three typical surface textures of fish scale trajectories

when $A = f_z/2$, the adjacent tool trajectories fluctuate and the crest (valley) of the former tool tooth coincides with the valley (crest) of the next tooth, which forms the second type of fish scale surface texture as shown in Fig.3 (b). The characteristic dimensions can be obtained as:

$$\begin{cases} \widehat{AB}=\pi rn/60f_x \\ CD=2A_x \end{cases} \quad (8)$$

when $\frac{f_z}{2} < A < f_z$, the trajectory of the crest (valley) of the former tool tooth overlap with the valley (crest) of the current tool trajectory, which forms the third type of fish scale surface

texture as shown in Fig. 3 (c). The geometric parameters of the surface texture can be expressed by Eq.(9), and it can be found that the second type surface texture is a specific case of the third type, when $A=f_z/2$.

$$\begin{cases} \widehat{AB} = \pi rn/60f_x \\ CE = FD = A_x - f_z/2 \\ EF = 2f_z \\ CD = 2A_x + f_z \end{cases} \quad (9)$$

It can be noted that the length $\widehat{\mathrm{AB}}$ of the surface texture is proportional to the tool radius and the spindle speed, while, inversely proportional to the vibration frequency. The width CD of the surface texture increases with the increase of the feed per tooth and the amplitude of the vibration.

3. Vibration stage design

In order to realize vibration assisted milling, a 2D vibration stage is designed, fabricated and tested. The design configuration of the stage is of important for the performance of vibration stage. Several design configurations of 2D vibration stage for vibration assisted machining have been developed and are summarized below. Zhang et al. [19] developed a vibration stage as shown in Fig. 4(a), where two piezoelectric actuators generate 2D vibration to the objective table. The planar integrated structure has the characteristics of compact structure, zero clearance and no mechanical friction. The piezoelectric actuators in x direction increases the mass of the vibration stage, thus, the vibration frequency in y direction is restricted, usually less than 1000 Hz. An improved 2D vibration stage was developed by Jin et al. [20], as shown in Fig.4 (b). The piezoelectric actuators are set beside the hinge part, which transforms vibration to the workpiece access the flexure hinges in x and y directions. The piezoelectric actuator can generate the vibration to the vertical direction flexure hinges, but in

the horizontal direction, the flexure hinge will be affected by the coupling stiffness, hence the displacement of the platform will be uneven. Therefore, it is difficult to control the displacement of the platform precisely. Li et al. [21] developed a 2D vibration stage by using a single flexure four bar mechanism, but when the single flexure parallel four bar mechanism vibrates at one direction, there will exist a cross-coupling displacement in another direction, which reduces the motion accuracy, as shown in Fig.4 (c). Different to the typical 2D vibration solutions based on the flexure mechanism driven by piezo-actuators, Chang et al. [22] reported a vibration table employing piezo-actuators in conjunction with two slideways for generating the desired two-dimensional vibration, as shown in Fig.4 (d).

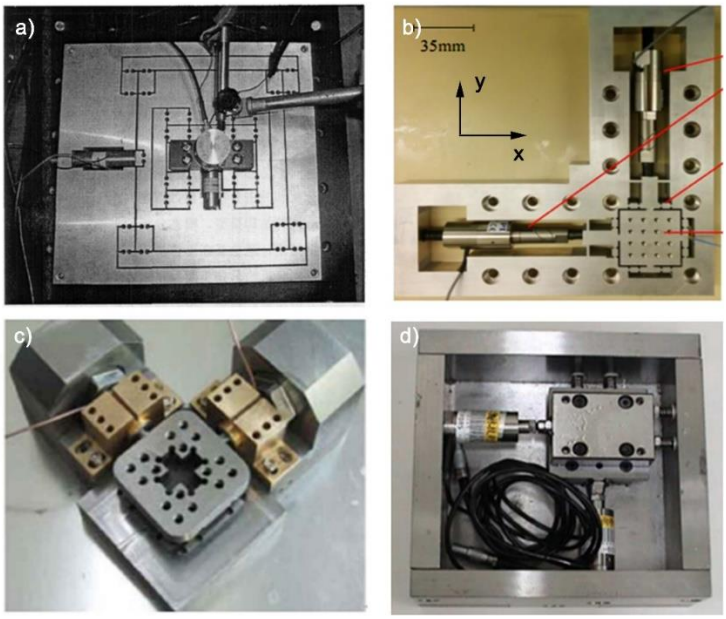

Fig. 4. Typical structures of vibration stage for vibration assisted milling [23]

Based on the design configurations discussed above, a novel structure of 2D vibration stage is proposed in this paper. As shown in Fig.5, two layers of flexure hinges are adopted in the vibration structure. The outer layer flexure hinges guide the vibration in x and y direction, while the inner layer flexure hinges reduce the displacement couple effect in x and y direction.

The outer and inner parts are combined with each other so that the vibration can transform effectively. This structure design adopts the advantages of the former designs and resolves the issues abovementioned.

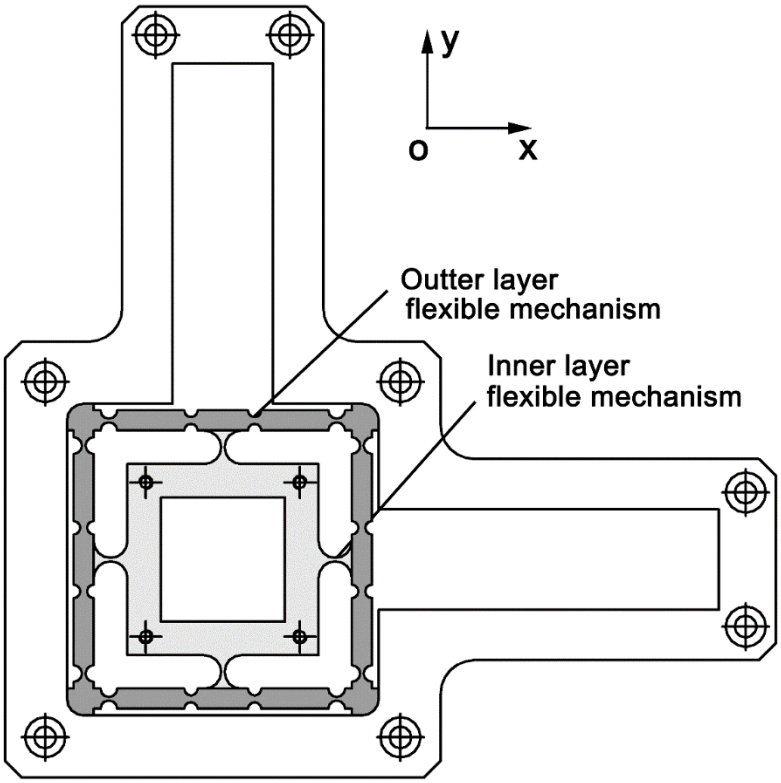

Fig. 5. Structure of the designed vibration stage

The designed structure of the vibration stage in x and y direction can be equivalent to a double four connecting rod flexure mechanism in the outer layer, as shown in Fig.6 and a single rod flexure mechanism in the inner layer, as shown in Fig.7.

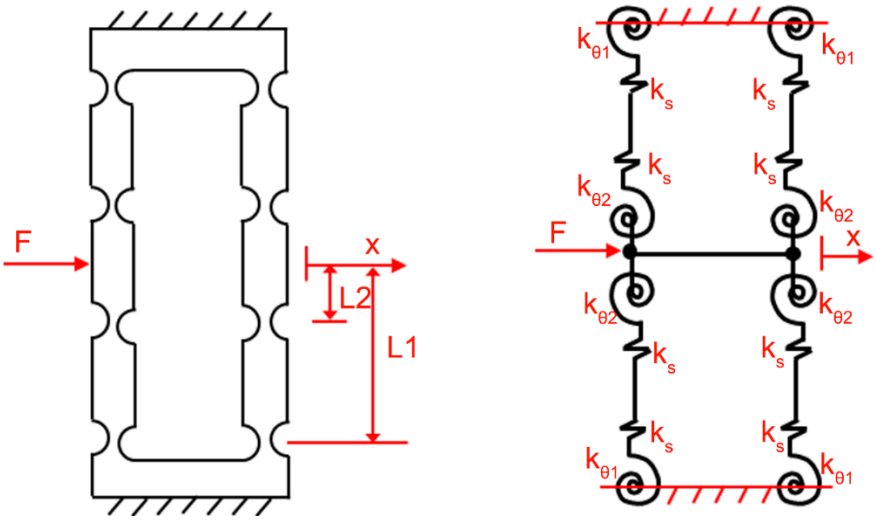

Fig.6 Diagram illustrating a double flexure hinge

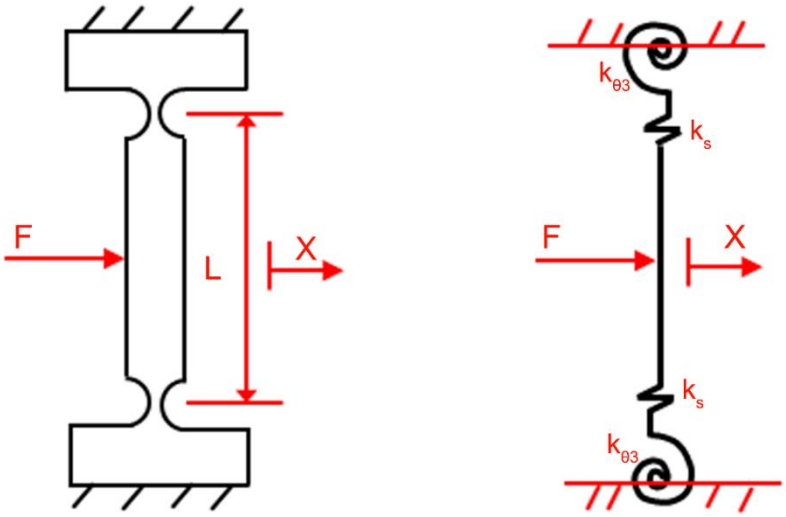

Fig.7 Diagram illustrating a single flexure hinge

3.1 Dynamic analysis of the vibration stage

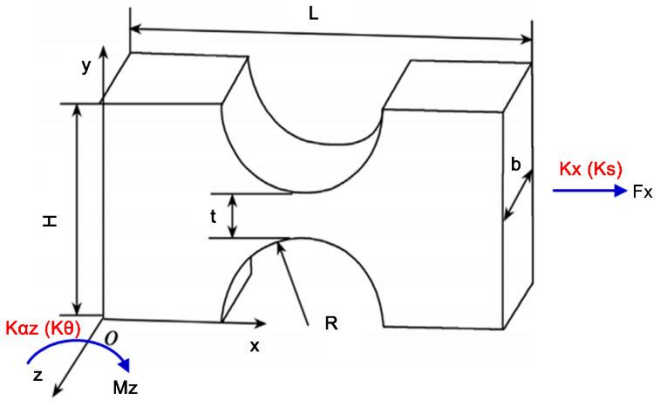

Fig.8 schematic diagram of a circular flexure hinge

Fig.8 shows the schematic diagram of a circular flexure hinge. The main functional motion of the flexure hinge is the rotation around the *z* axis, and the stretch along the *x* axis. Therefore, the respective stiffness $K_{\alpha z}$ and K_x should be calculated.

Assume the flexure hinge is fixed at one end. Loading force F_x, and bending moment M_z are applied at the other end. The angular displacement caused by the moment M_z is relatively small, hence it can be expressed as:

$$\theta \approx tan\,\theta = \frac{dy}{dx} \tag{10}$$

The deformation of a single-axis flexure hinge could be considered as the sum-up of a chain of micro segments, and each segment is equivalent to a uniformed beam with the section area dx. The moment at both ends of the segment is equal to one another.

Radius of the curvature, ρ, in the flexure hinges is obtained by:

$$\frac{1}{\rho} = \frac{M(x)}{EI(x)} \tag{11}$$

where *E* is the elastic modulus, *M(x)* represents the bending moment over dx, and I(x) is the 2nd moment of area.

The relation between angular stiffness and angular displacement α_z caused by the bending moment M_z is expressed as:

$$K_\theta = \frac{M_z}{\alpha_z} = \frac{EbR^2}{12\left[\frac{2s^3(6s^2+4s+1)}{(2s+1)(4s+1)^2}+\frac{12s^4(2s+1)}{(4s+1)^{5/2}}\tan^{-1}\sqrt{4s+1}\right]} \tag{12}$$

And the relation between axial stiffness and axial displacement Δx caused by Fx is expressed as:

$$K_s = \frac{F_x}{\Delta x} = \frac{Eb}{\left[\frac{2(2s+1)}{\sqrt{4s+1}}\tan^{-1}\sqrt{4s+1}-\frac{\pi}{2}\right]} \tag{13}$$

where s=R/t. b, t, and R are annotated in Fig. 8.

3.1.1 Stiffness of the double four connecting rod flexure mechanism of the outer layer

Assume the flexural stiffness of the flexure hinge is $k_{\theta 1}$ and $k_{\theta 2}$, then when the double four link mechanism produces the displacement of S under the action of external force F, the elasticity of each flexure hinge is

$$W_{\theta i} = \frac{1}{2} k_{\theta i} \theta^2 \qquad (14)$$

where $\theta = \frac{S}{L_1 - L_2}$ (15)

The work done by the force is:

$$W = \frac{1}{2} FS \qquad (16)$$

Ignore the energy loss, e.g. heat generation:

$$W = \sum_{i=1}^{8} W_{\theta i} \qquad (17)$$

Thus, the stiffness of the of the double four connecting rod flexure mechanism in the outer ring can be expressed as:

$$K_{outer} = \frac{4(k_{\theta 1} + k_{\theta 2})}{(L_1 - L_2)^2} \qquad (18)$$

L_1, L_2, $k_{\theta 1}$ $k_{\theta 2}$ are annotated in Fig. 7 a).

3.1.2 Stiffness of the single rod flexure mechanism of inner ring

Assume the stiffness of the flexure hinge is $k_{\theta 3}$, then when the double four link mechanism produces the displacement of S under the action of external force F, the elasticity of each flexure hinge is：

$$W_{\theta 3} = \frac{1}{2} k_{\theta 3} \theta^2 \qquad (19)$$

where

$$\theta = \frac{S}{L} \qquad (20)$$

The work done by the force is

$$W = \frac{1}{2}FS \qquad (21)$$

Ignore the energy loss, e.g. heat generation:

$$W = 2W_{\theta i} \qquad (22)$$

Thus, the stiffness of the single rod flexure mechanism of inner ring can be expresses as:

$$K_{inner} = \frac{2k_{\theta 3}}{L^2} \qquad (23)$$

The total stiffness, K_{total} and the natural frequency, ω_n of the vibration stage in x direction can be obtained:

$$K_{total} = K_{outer} + K_{inner} \qquad (24)$$

$$\omega_n = \frac{1}{2\pi}\sqrt{\frac{K_{total}}{M}} \qquad (25)$$

The total stiffness and natural frequency of the designed vibration stage in x and y direction are shown in Table 1.

Table 1 the structural properties of the designed vibration stage

Parameters	$k_{total-x}$	ω_{nx}	$k_{total-y}$	ω_{ny}
Value	50 N/μm	3269 Hz	50 N/μm	3269 Hz

Two preloaded piezo actuators (P-844.20 Physik Instrumente) are selected to drive the vibration stage, and their specifications are given in Table 2.

Table.2 The specifications of P-844.20 piezo actuators

Travel range	30μm	Electrical capacitance	12μF
Resolution	0.3nm	Resonant frequency	12 KHz
Stiffness	107 N/μm	Mass without cable	108g
Push/Pull force	3000N	Length	65mm

The actual achievable displacement of the platform is:

$$\Delta L = \Delta L_0 \frac{K_a}{K_a + K_x} \qquad (26)$$

where $K_a = 107\mathrm{N/\mu m}$ is the stiffness of the piezo-actuator, ΔL and ΔL_0 represent the displacement of the platform and the stroke of the actuator, respectively. Therefore, the

maximum displacement is determined to be 20μm.

3.2. Control system design and vibration relationship

In the designed stage, the piezoelectric actuators that convert electrical energy to linear motion with the features of high precision, large driving force and fast response are responsible for stage vibration generation. A LabVIEW program is used for the control of the vibration stage and data acquisition. Fig. 9 shows the schematic of the machine tool and vibration stage control system. The control signals, are set by a host computer and amplified through a high voltage piezo amplifier, and then are used to drive the piezo actuators. Meanwhile, the stage displacement data is fed back to the host computer through data acquisition cards for recording. Prior to installation of the vibration stage, its performance is tested on a metrology table as shown in Fig. 10. A modular capacitive sensor system (DL6220, Micro-epsilon) and two capacitive sensors (CS005, Micro-epsilon) with 1nm resolution and 50 μm measuring range are used to measure the displacement in both directions.

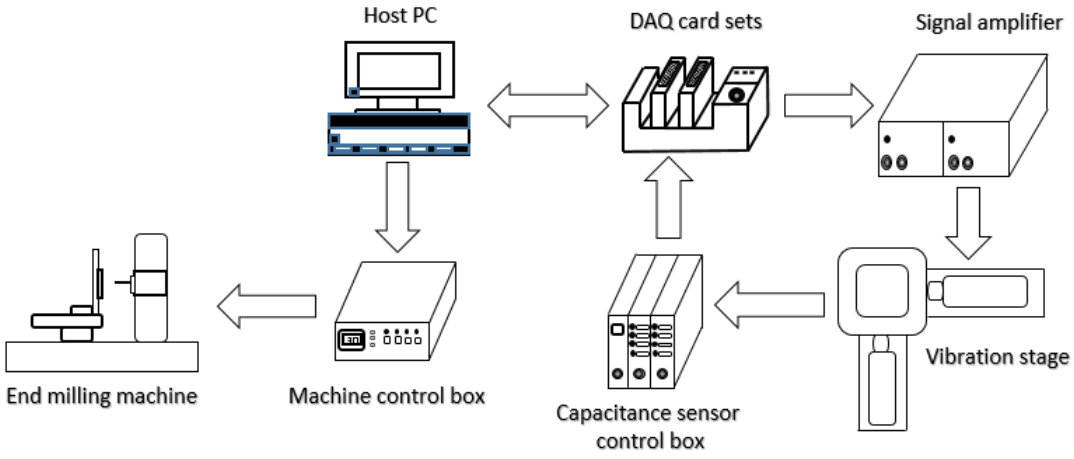

Fig.9 Schematic of the machine tool and vibration stage control system

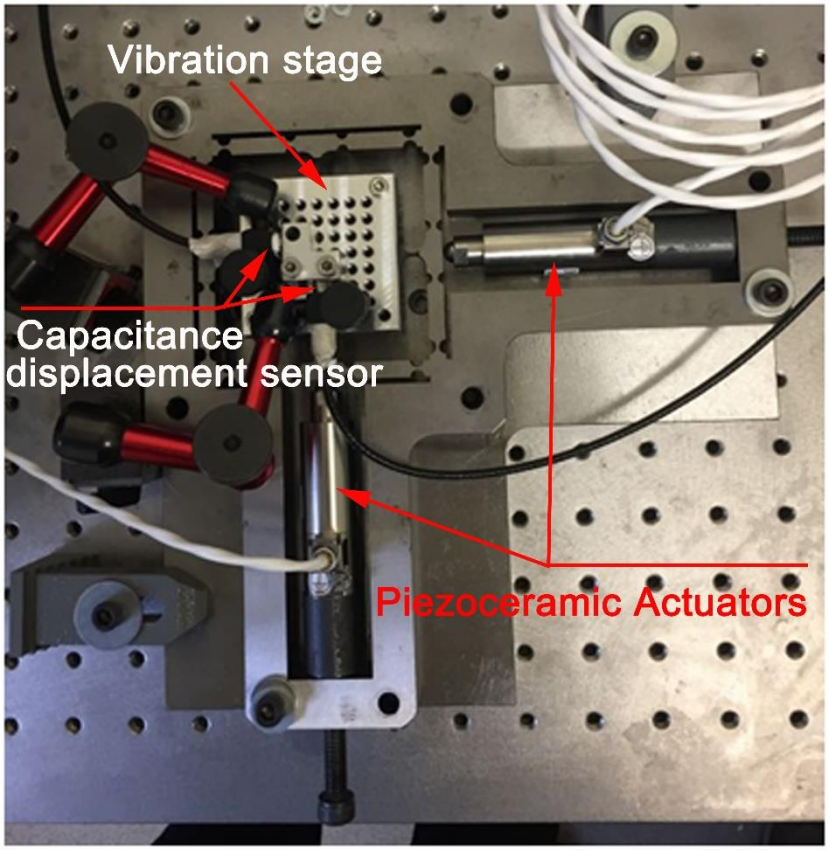

Fig.10 Layout of the testing devices

In the VAM control process, vibration trajectory errors are unavoidable because the stage manufacturing errors, electronic devices interference and control signal distortion. Fig. 11 shows an example of the testing results, where two voltage signals (0.2V, 1000Hz) with 90° phase difference are sent into the system. A total vibration trajectory error of 0.25 μm is measured. In the subsequent vibration assisted machining experiment, these errors are compensated by the programme to achieve demanded vibration displacement.

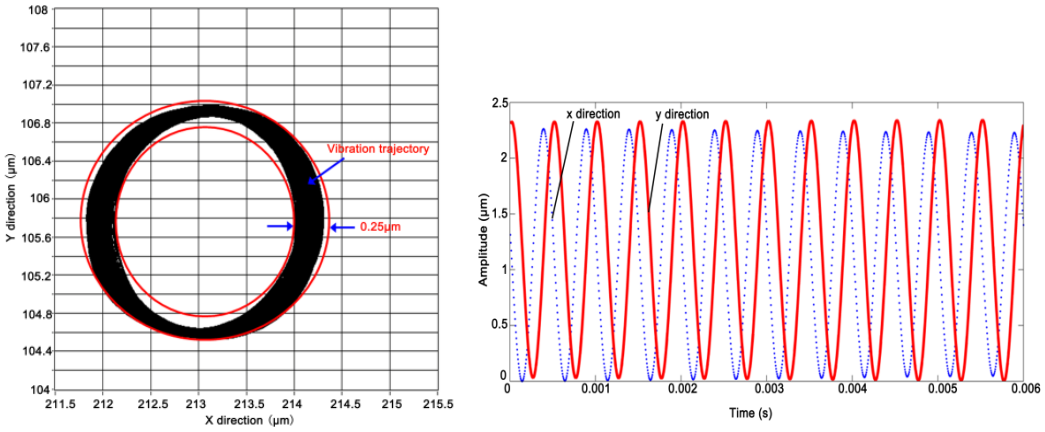

Fig. 11 Error test results

4. Surface texture machining experiments and hydrophilic testing

4.1 Machining experiments

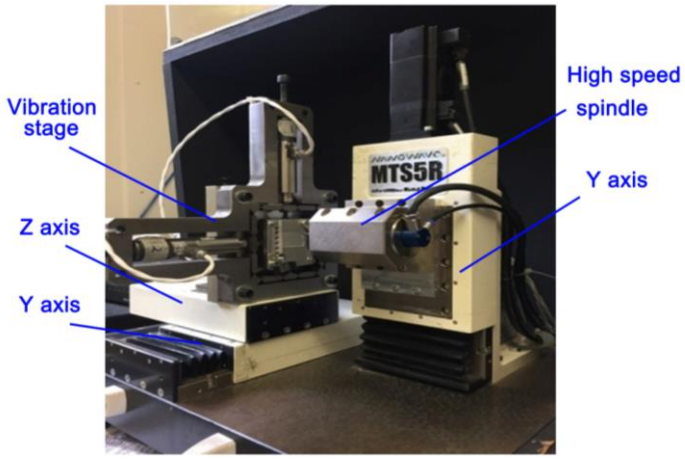

Fig. 12 Layout of testing equipment

The designed vibration stage is installed on a three axis micro milling machine tool, as shown in Fig.12. To validate the surface texture simulation in Section 2, machining tests were carried out using 0.5 mm diameter uncoated two flute micro end mills. Al 6061-T6 workpiece material is used in order to reduce the influence of tool wear.

The experiments are carried out with four sets of machining and vibration parameters as given in Table 3, the ratio between the vibration frequency and the spindle rotation frequency is 0, 10, 11 and 17, respectively.

Table 3 Machining and vibration parameters

No.	Spindle speed (rpm)	Vibration frequency (Hz)	Vibration amplitude (μm)	Feed per tooth (μm)	Depth of cut (μm)
Set 1	12,000	0	0	5	10
Set 2	12,000	2,000	2.5	5	10
Set 3	12,000	2,200	2.5	5	10
Set 4	12,000	3,400	2.5	5	10

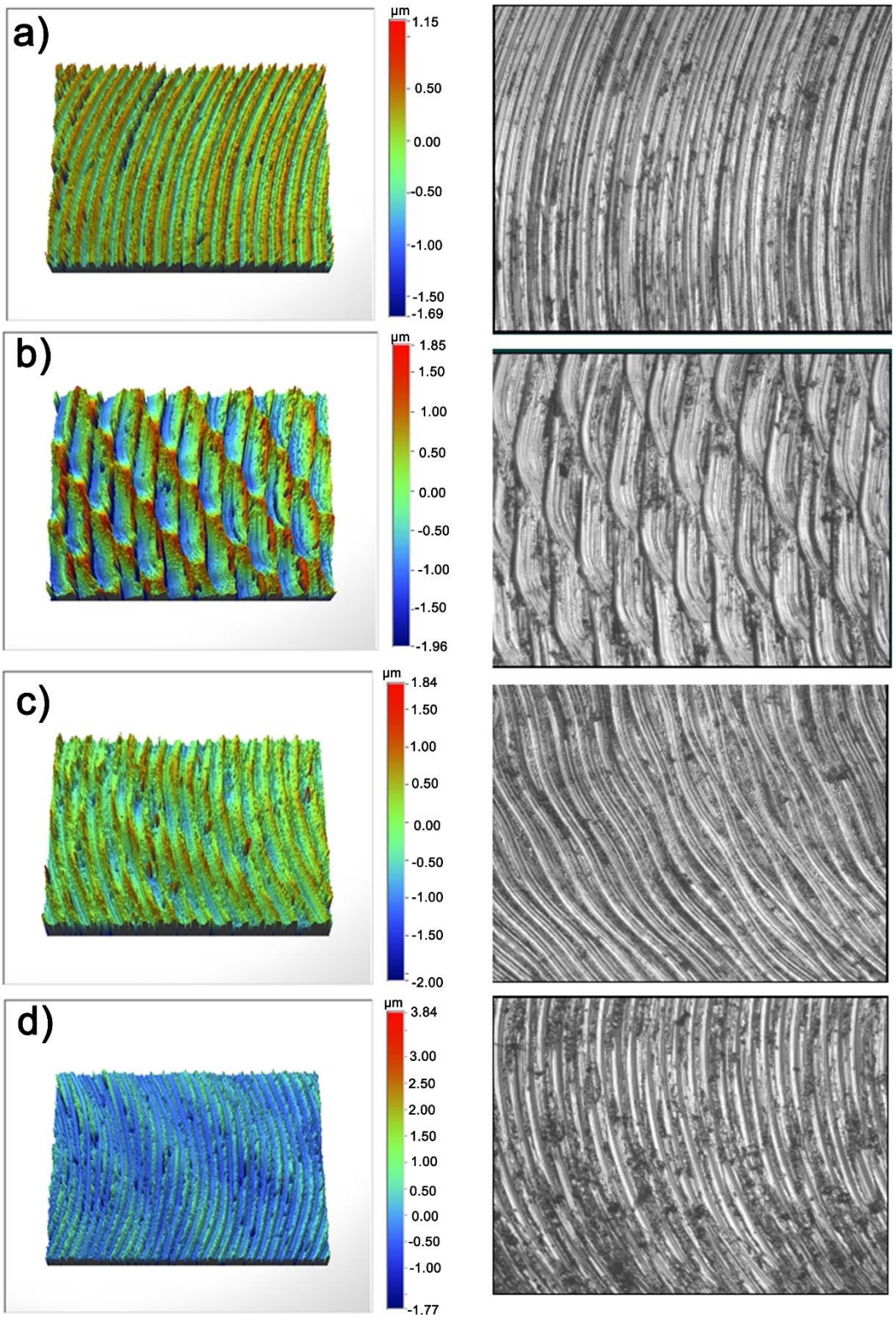

Fig. 13 Machined surface textures results from vibration assisted milling. Machining conditions: a) Set 1 (without vibration assistance); b) Set 2; c) Set 3; d) Set 4

The surface texture measurement results from four sets of machining parameters are shown in Fig.13. Fig.13 (a) shows the surface generated by the conventional micro milling without vibration assistance. Clear regular circular tool marks are observed. Fig.13 (b) illustrates the surface texture of the machined surface with the 2nd set machining/vibration parameters, i.e. the vibration frequency is 10 times of the spindle rotation frequency, and the vibration amplitude is half of the feed per tooth. It can be observed that the trajectories of the tool vibration are along the cutting path, and the crest (valley) of one tooth overlaps with the valley (crest) of another tooth exactly, which forms the second type fish scale texture on the machined surface as predicted in the simulation. Fig.13(c) and (d) illustrates the surface texture of the machined surface with the 3rd and 4th sets machining/vibration parameters, i.e. the vibration frequency are 11 times and 17 times of the spindle rotation frequency. It can be observed that the trajectories of the tool vibration are along the cutting path, and the crest (valley) of one tooth corresponds to the crest (valley) of another tooth, which forms the wave type textures on the machined surface as predicted in the simulation.

The machined surface texture results agree well with the analytical predications for the two flute end mills. When the vibration frequency is even times of the spindle rotation frequency, the fish scale type textures are formed on the machined surface. When the vibration frequency is odd times of the spindle rotation frequency, the wave type texures are formed on the machined surface. The results show that vibration assisted micro milling provides a new controllable and efficient method for generating certain surface textures over reletively large surface area.

4.2 Hydrophilic test

Designing surface hydrophilicity performance is desirable for many applications. This section studies the wettability of different surface textures generated by the vibrated assisted milling to demonstrate an application of such surface textures. The water contact angle of the 3D machined surfaces was measured by a Sindatek Water Contact Goniometer with 5 ml water droplets. Fig. 14 (a) shows the surface texture from conventional micro milling using the 1st set machining parameters without vibration assistance and it can be observed that the water contact angle is 89°, which indicates a hydrophobic surface. Then, water contact angles of the surfaces machined by vibration assisted milling were compared to analyze the effect of vibration parameters on the wettability of the surfaces. Fig.14 b)-d) show that the water contact angle measurement of three typical surfaces textures generated with different machining/vibration parameters (the 2nd - 4th set parameters in Table 3). The results show that the waviness has the effect to increase the wettability, with the decrease of the waviness period the water contact angle shows a decreasing trend. However, when the surface texture changes to fish scale structure, the water contact angle was significantly reduced from 89° to 30°, the surface changes to super hydrophilic surface. Thus, controllable wettability of the machined surface can be realized by combining different machining and vibration parameters. It is very desirable to control the wettability of the machined surface, e.g. in microfluidic channels, different region needs different wettability to control the flow rate and mixing efficiencies of different fluids. Conventional processing methods are difficult to achieve controllable wettability, while vibration assisted milling provides a viable solution for such applications.

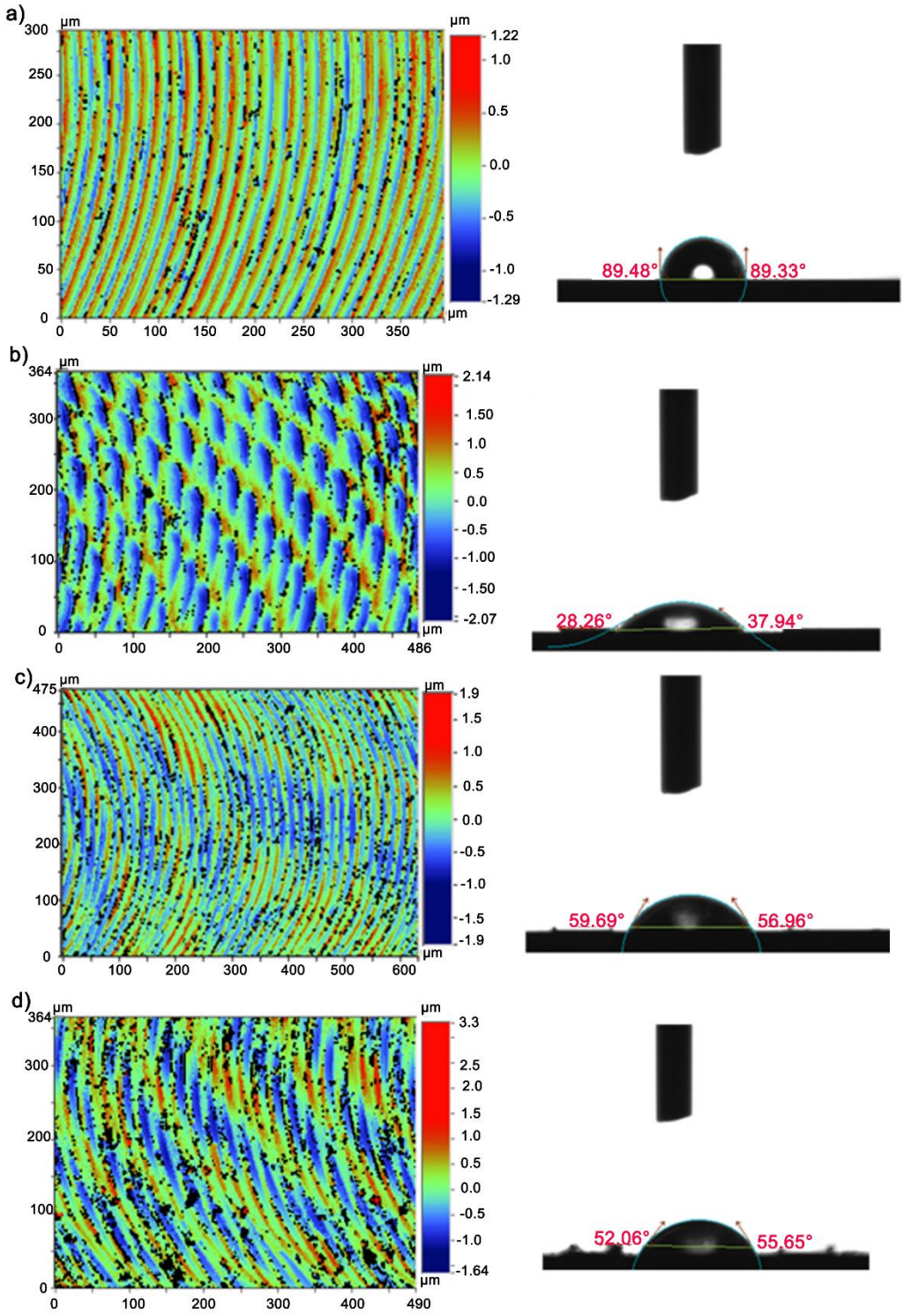

Fig.14 Wettability of the different topography, Machining conditions: a) Set 1 (without vibration assistance); b) Set 2; c) Set 3; d) Set 4

5. Conclusion

The surface texture formation by non-resonant vibration assisted micro milling is presented in

this paper. The effect of vibration and machining parameters on the surface texture generation are investigated based on the kinematic analysis and machining experiments. The following conclusions can be drawn:

- Two specific types of surface textures – wave and fish scale can be generated by using appropriate machining and vibration parameter sets. The ratio between the vibration frequency and the spindle frequency have significant influence on the surface texture formation.
- Controllable wettability of the machined surface can be realized by combining different machining parameters. The machined surface texture results agree well with the analytical predications for the two flute end mills.
- The wettability test results on the machined surface show that vibration assisted micro milling can be used for generation of specific surface textures and designing hydrophobicity surface property.

Acknowledgment

The authors gratefully acknowledge financial support of the Engineering and Physical Sciences Research Council (EP/M020657/1), the National Natural Science Foundation of China (Grant No.51505107), and Project (HIT.NSRIF.2017029) supported by Harbin Institute of Technology.

Conflict of interest

The authors declare that there is no conflict of interest.

Reference:

[1] Jung, Yong Chae, and Bharat Bhushan. "Contact angle, adhesion and friction properties of

micro-and nanopatterned polymers for superhydrophobicity."*Nanotechnology* 17.19 (2006): 4970.

[2] Maboudian, Roya, and Roger T. Howe. "Critical review: Adhesion in surface micromechanical structures." *Journal of Vacuum Science & Technology B: Microelectronics and Nanometer Structures Processing, Measurement, and Phenomena* 15.1 (1997): 1-20.

[3] Liao, H., B. Normand, and C. Coddet. "Influence of coating microstructure on the abrasive wear resistance of WC/Co cermet coatings." *Surface and Coatings Technology* 124.2 (2000): 235-242.

[4] Alpas, A. T., and J. Zhang. "Effect of microstructure (particulate size and volume fraction) and counterface material on the sliding wear resistance of particulate-reinforced aluminum matrix composites." *Metallurgical and Materials Transactions A* 25.5 (1994): 969-983.

[5] Kanemitsu, Yoshihiko, et al. "Microstructure and optical properties of free-standing porous silicon films: Size dependence of absorption spectra in Si nanometer-sized crystallites." *Physical review B* 48.4 (1993): 2827.

[6] Hadad, Mohammadjafar, and Mohammadjavad Ramezani. "Modeling and analysis of a novel approach in machining and structuring of flat surfaces using face milling process." *International Journal of Machine Tools and Manufacture* 105 (2016): 32-44.

[7] P. Wilkinson, R.L. Reuben, J.D.C. Jones, J.S. Barton, D.P. Hand, T.A. Carolan, S.R. Kidd, Surface finish parameters as diagnostics of tool wear in face milling,Wear 205 (1997) 47–54.

[8] Takahata KI, Gianchandani YB. (2002) Batch mode micro-electro-discharge machining.

J. Microelectromechanical Systems, 11(2):102-110.

[9] Derevyanko, D. I., et al. "Fabrication of High-aspect-ratio Microstructures for LIGA-technology by Sinchrotron Radiation Polymerisation of Thetetraacrylate Monomer." *Physics Procedia* 86 (2017): 122-126.

[10] Chen, Kexun, et al. "Novel texturing process for diamond-wire-sawn single-crystalline silicon solar cell." *Solar Energy Materials and Solar Cells* 133 (2015): 148-155.

[11] Tong, Zhen, and Xichun Luo. "Investigation of focused ion beam induced damage in single crystal diamond tools." *Applied surface science* 347 (2015): 727-735.

[12] Venugopal, Gunasekaran, Sang-Jae Kim, and Shrikant Saini. *Focused Ion Beam Based Three-Dimensional Nano-Machining*. INTECH Open Access Publisher, 2012.

[13] Zimmer, K., D. Hirsch, and F. Bigl. "Excimer laser machining for the fabrication of analogous microstructures." *Applied surface science* 96 (1996): 425-429.

[14] Tong, Z., Xu, Z., Wu, W., and Luo, X. (2015). Molecular dynamic simulation of low-energy FIB irradiation induced damage in diamond. *Nuclear Instruments and Methods in Physics Research Section B: Beam Interactions with Materials and Atoms*, *358*, 38-44.

[15] Zheng ZP, Cheng WH, Huang FY, Yan BH. (2007) 3D microstructuring of Pyrex glass using the electrochemical discharge machining process. J. Micromechanics and Microengineering, 17(5):960-966.

[16] Kim G, Loh B. (2011) Direct machining of micro patterns on nickel alloy and mold steel by vibration assisted cutting. Int. J. Prec. Engin. Manuf., 12(4):583-588.

[17] Kim G, Loh B. (2013) Cutting force variation with respect to tilt angle of trajectelliptical vibration V grooving. Int. J. Prec. Engin. Manuf., 14(10):1861-1864.

[18] Kim J, Lee S-K. (2006) Micro-patterning technique using a rotating cutting tool controlled by an electromagnetic actuator. Int. J. Machine Tools and Manufacture, 101:52-64.

[19] Zhang, J. and Sun, B. 2006Design and Analysis of 2-DOF Nanopositioning Stage Based on Dual Flexure Hinges. China Academic Journal Electronic Publishing House, 5(28).

[20] Jin X, Xie B. 2015Experimental study on surface generation in vibration-assisted micro-milling of glass. The International Journal of Advanced Manufacturing Technology, 81(1-4): 507-512.

[21] Li G. 2012Non-resonant vibration auxiliarytable development and study on micro-milling technology experiment [PhD thesis]. Harbin institute of technology.

[22] Chern G L, Chang Y C. 2006 Using two-dimensional vibration cutting for micro-milling. International Journal of Machine Tools and Manufacture. 46(6): 659-666.

[23] Huo, D., Chen, W., Lin, L., Zheng, L. and Hale, J. Development of a high bandwidth XY stage for vibration-assisted milling. Proceedings of 17th International Conference of the European Society for Precision Engineering and Nanotechnology, Hannover, Germany, 2017